

Ab initio calculation of anisotropic interfacial excess free energies

A. van de Walle, Q. Hong, and L. Miljacić
*Brown University**

C. Balaji Gopal, S. Demers, and G. Pomrehn
Caltech

A. Kowalski
Google

P. Tiwary
ETHZ
(Dated: April 24, 2014)

We describe a simple method to determine, from ab initio calculations, the complete orientation-dependence of interfacial free energies in solid-state crystalline systems. We illustrate the method with an application to precipitates in the Al-Ti alloy system. The method combines the cluster expansion formalism in its most general form (to model the system's energetics) with the inversion of the well-known Wulff construction (to recover interfacial energies from equilibrium precipitate shapes). Although the inverse Wulff construction only provides the relative magnitude of the various interfacial free energies, absolute free energies can be recovered from a calculation of a single, conveniently chosen, planar interface. The method is able to account for essentially all sources of entropy (arising from phonons, bulk point defects, as well as interface roughness) and is thus able to transparently handle both atomically smooth and rough interfaces. The approach expresses the resulting orientation-dependence of the interfacial properties using symmetry-adapted bases for general orientation-dependent quantities. As a by-product, this paper thus provides a simple and general method to generate such basis functions, which prove useful in a variety of other applications, for instance to represent the anisotropy of the so-called constituent strain elastic energy.

I. INTRODUCTION

Interfacial free energies play an important role in the design of engineering materials, as they represent a fundamental determinant of microstructure^{1,2}. However, the experimental measurement of interfacial free energies can represent a difficult challenge^{3–6} and computational approaches have thus proven useful to provide complementary corroborating estimates^{1,7–13}.

The two main challenges faced when determining interfacial properties via computational means are that (i) the interface structure may take considerable time to equilibrate and that (ii) at finite temperature, defects are present in thermodynamic equilibrium, a situation which typically requires sampling of numerous possible microscopic states. This situation prompts for the use of computationally very efficient energy models. In the case of coherent interfaces, the cluster expansion formalism¹⁴ has been proven a very effective approach to the simulation of interfaces^{9–13,15–20}. The cluster expansion provides a very compact and systematically improvable representation of the configurational-dependence of an alloy's energy and the process of constructing such a cluster expansion (with a given accuracy) from ab initio data is well-established²¹.

While it is common to proceed by studying planar interfaces one direction at a time in a supercell geometry, there are compelling reasons to proceed by considering all interface directions in a single large-scale simulation. This can be useful to directly determine equilibrium precipitate shapes (e.g.¹³). More generally, such a global approach proves most useful for the determination of interface free energies if (i) the thermodynamically stable directions are not known a priori or if there may be a continuum of stable directions when temperature is sufficiently high and the interfaces roughen or (iii) if the determination of the complete orientation dependence of the interfacial free energy is needed. The latter is especially useful to provide input to continuum-type simulations, such as phase field^{22–24} or finite element²⁵ modeling.

This paper describes a simple method to determine, from ab initio calculations, the complete orientation-dependence of interface free energies in solid-state crystalline systems. The method combines the cluster expansion formalism in its most general form (to model the system's energetics) with the inversion of the well-known Wulff construction^{26–28} to recover interfacial energies from equilibrium precipitate shapes. Although the inverse Wulff construction only provides the relative magnitude of the various interfacial free energies, absolute free energies can be recovered from a calculation of a single, conveniently chosen, planar interface (although not necessarily flat at the atomic level). The method is able to account for essentially all sources of entropy (arising from phonons, bulk point defects, as well

as interface roughness) and is thus able to transparently handle both atomically smooth and rough interfaces. To address the issue that some interface directions do not appear on the Wulff shape when the facetting occurs, we show how the interfacial free energy surface can be naturally extended into the “masked” regions of the Wulff plot in a way that (i) preserves the predicted equilibrium shape and (ii) has a natural geometric interpretation. The approach finally expresses the resulting orientation-dependence of the interfacial properties using symmetry-adapted bases for general orientation-dependent quantities. As a by-product, this paper thus provides a simple and general method to generate such basis functions, which prove useful in a variety of other applications, for instance to represent the so-called constituent strain elastic energy of superlattice structures in the long wavelength limit^{29,30}. The proposed method can be easily implemented using generic linear algebra operations without having to consider many different subcases that depend on the point group symmetry considered. The method exploits a direct correspondence between spherical harmonics and polynomial functions of a unit vector expressed in tensor notation. The methods proposed herein have been implemented within the Alloy Theoretic Automated Toolkit (ATAT)^{21,31–33}.

As an example to demonstrate the method, we select the Ti-Al alloy system because it exhibits a number of interesting and challenging features. Al₃Ti precipitates in an Al-rich fcc host exhibiting a D0₂₃ structure which has a relatively low symmetry (thus increasing the number of distinct facets). We also find that such precipitates exhibit a mixture of atomically smooth and rough facets at all but the lowest temperatures. Moreover, previous work has shown that vibrational contributions to the free energy in this alloy are large^{34–36} and must therefore be included in the assessment of interfacial boundary energies.

II. METHODS

A. Coarse Graining Cluster Expansion

The system considered here consists of coherent precipitates within a host phase with a known lattice type (fcc). For efficiency reasons, we select a form of energy model especially adapted to this situation. The approach to the determination of interface free energies is not tied to this specific energy model, however. We rely on the cluster expansion formalism^{14,37–39}, which represents the energy E of a crystalline alloy with a computationally efficient Hamiltonian taking the form of a polynomial in terms of occupation variables $\sigma_i = \pm 1$ indicating the type of atom residing on each lattice site i :

$$E = \sum_{i \neq j} J_{ij} \sigma_i \sigma_j + \sum_{i \neq j \neq k} J_{ijk} \sigma_i \sigma_j \sigma_k + \dots \quad (1)$$

The unknown coefficients, J_{\dots} , of this polynomial are called Effective Cluster Interactions (ECI) and are fit to a database of *ab initio* structural energies (obtained from Density Functional Theory total energy calculations). It has been formally shown that an infinite series of this form can represent any configuration-dependence of the energy¹⁴. Moreover, formal methods have been developed to determine the number of terms and the database size needed to achieve a given precision²¹. The ECI can typically be determined from a reasonably-sized database of ab initio calculations involving small-unit-cell atomic arrangements. These ECI can then be used in a large-scale equilibrium Lattice-Gas Monte Carlo simulations of the coherent interface, without necessitating repeated large-scale ab initio calculations for each atomic configuration visited in a thermodynamic equilibrium. These tasks were carried out with the help of the Alloy Theoretic Automated Toolkit (ATAT)^{21,31–33}.

The effect of lattice vibrations can be included within this framework, via a coarse-graining technique⁴⁰. The idea is to replace, in Equation (1), the energy E by the phonon contribution to the free energy for a given configuration σ . The resulting effective interactions J_{\dots} now become temperature-dependent, but the formalism otherwise remains the same. As full lattice dynamics calculations can be computationally expensive to repeat for numerous configurations σ , we rely on the “bond stiffness vs bond length” approach^{40,41}. In this approach, the effective springs connecting nearby atoms are calculated for a few structures only for a range of lattice parameters. The data thus generated is used to determine the relationship between the stiffness of an effective spring and the distance between the corresponding pair of atoms. Once this is known, the relaxed atomic position for all remaining structures (obtained from the ab initio calculations) can be used to predict spring constants without necessitating additional ab initio lattice dynamics calculations.

The above cluster expansion deliberately does not include long-range elastic effects, because we wish to determine the chemical and local relaxations contribution of the interface, and not the strain energy associated with deforming the host and the precipitate due to their coherent coexistence. Had we included so-called constituent strain effects^{29,30} in (1), we would have had to later subtract elastic energies via a continuum elasticity-type analysis. One should however be cautious not to interpret the equilibrium precipitate shape found in our simulations as the actual equilibrium

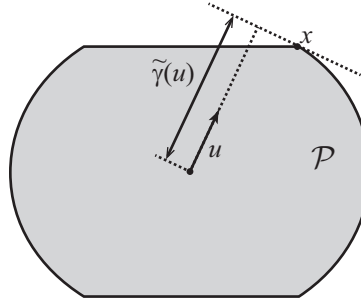


FIG. 1: Graphical representation of the inverse Wulff construction defined by Equation (2).

precipitate shape (which is affected by elastic effects). However, the equilibrium precipitate shape we obtain is the relevant shape for the purpose of determining the interfacial excess free energy, independently of long-range elastic effects. For simplicity of the presentation we nevertheless use the phrase “equilibrium precipitate shape” throughout, with the understanding that elastic effects are omitted, as they should for a purely interfacial analysis. It should be observed that, in the limit of small precipitates, interfacial effects (scaling as r^2 for precipitates of length scale r) dominate over elastic effects (scaling as r^3), so our equilibrium precipitate shapes should nevertheless be representative of actual precipitate shapes in this $r \rightarrow 0$ limit.

B. Ab initio calculations

All ab initio calculations were performed with the VASP code^{42,43} implementing the Projector Augmented Wave (PAW) method⁴⁴. The PBE exchange-correlation functional⁴⁵ was used. The kinetic energy cutoff was set to 300 eV (corresponding to VASP’s “high” precision setting). The k-point mesh was set via the algorithm described in²¹ to ensure a density of at least 8000 k-points per (atom)⁻¹ for all superstructures considered. For the large-supercell phonon calculations, these settings were reduced 240 eV (corresponding to VASP’s “medium” precision setting) and 4000 k-points per (atom)⁻¹, respectively.

C. Inverse Wulff construction

The Wulff construction^{26,27} is a well-known procedure to calculate the equilibrium precipitate shape from the directional-dependence of the interfacial excess free energy. This procedure can be readily inverted (see, e.g.²⁸) to yield the interfacial excess free energy from the knowledge of the equilibrium precipitate shape. Let $\gamma(u)$ denote the interface free energy with an orientation defined by some unit vector u . Let \mathcal{P} denote a set in three-dimensional space representing the shape of a precipitate in equilibrium. The inverse Wulff construction $\tilde{\gamma}(u)$ is illustrated in Figure 1 and is given by

$$\tilde{\gamma}(u) = \max_{x \in \mathcal{P}} u \cdot x. \quad (2)$$

It follows directly from the Wulff construction that, for any facet u part of the equilibrium precipitate shape,

$$\gamma(u) = c\tilde{\gamma}(u), \quad (3)$$

where c is a multiplicative constant independent of direction u . What is less clear is the interpretation of (2) for directions u that do not correspond to equilibrium facets. From the Wulff construction, one can only conclude that $\gamma(u)$ is the minimum fictitious interface free energy that facet u could have without changing the Wulff shape. However, as shown in Appendix B, $\gamma(u)$ nevertheless has a clear physical interpretation: It is the surface free energy of a macroscopically flat surface with normal u but that is, at the microscopic level, made of facets from the Wulff shape. These facets are big enough so that the edge energies are negligible relative to the surface energies, but small enough so that the interface still appears macroscopically flat. Thus, the inverse Wulff construction $\gamma(u)$ automatically extrapolates the surface free energies to the “unstable” directions in a physically plausible fashion.

The determination of the precipitate shape \mathcal{P} from the Monte Carlo configuration snapshots typically requires the use of a suitable order parameter to identify which points belong or not to the precipitating phase. In the special case of precipitates forming from a dilute solid solution on the parent lattice, one can simply use the species that is dilute

(call it “D”) in the solid solution phase as a marker for the presence of the precipitating phase. One can easily screen out the solutes in solution by counting, for each D atom, the number of other D atoms in their vicinity and eliminating any D atom with an insufficient number of neighbors. The remaining D atom (in concentrated environments) should nicely trace out the precipitate shape.

When using this approach, it must be verified that the precipitate size used is sufficiently large to ensure (i) a small Gibbs-Thomson effect^{46,47} (i.e. changes in chemical potential due to interface curvature) and (ii) a small ratio of the lattice parameter over the precipitate size. Note that the method is not sensitive to an overall direction-independent bias in interfacial free energies that could be due to the Gibbs-Thomson effect, because the inverse Wulff construction is only used to provide the relative values of the different interfacial free energies. Their overall direction-independent scale factor is determined by a separate calculation on a planar interface (described in the next section) that is therefore not affected by the Gibbs-Thomson effect. However, the Gibbs-Thomson effect could still affect the relative stability of two interface orientations through changes in equilibrium solute concentration, which in turn affect interface structures and their relative excess free energies. This effect is typically of a smaller magnitude than the isotropic component of Gibbs-Thomson-induced bias, but must still be carefully investigated. A second size issue arises from the fact that the lattice parameter places a lower bound on the “resolution” of our estimates of precipitate shape. Both the Gibbs-Thomson effect and the “resolution” bound scale as $1/r$, where r is of the order of precipitate “radius”.

D. Absolute interface free energies

In order to fix the arbitrary constant c in the inverse Wulff construction in Equation (3) we need to compute the absolute surface free energy for one facet. We have the freedom to pick a facet that simplifies the calculations. In this case, taking a facet that does not roughen proves useful, because the fluctuations in the interface structure are small, so that little Monte Carlo averaging is needed to obtain converged values.

In general (whether the chosen interface roughens or not), the interface free energy F_i can be calculated from the interface excess energy E_i by thermodynamic integration¹² of the relation $\partial(F_i/T)/\partial(1/T) = E_i$. To this effect, one can perform a sequence of lattice gas Monte Carlo simulations, starting from a perfectly atomically flat interface at $T = 0\text{K}$, where it is known that $F = E$, and integrating up to the desired temperature. Performing this procedure for various supercell periodicities (perpendicular to the interface), one can infer the contribution of the interface to the free energy. Alternatively, one can also use a Gibbs dividing surface construction to subtract appropriate amount of the free energy of the two bulk phases in contact from the total free energy of the supercell containing the interface. A natural choice of dividing surface is one that implies an excess solute concentration of zero.

In some systems, one can find an equilibrium facet that remains atomically flat up to the temperature of interest. This may happen when that interface’s low free energy is driven by a low interfacial energy rather than by a large interfacial entropy, i.e., when the energy associated with step formation is high. In this case, the thermodynamic integration process becomes redundant because there is no configurational contribution to the interfacial entropy. Hence, one can equivalently directly calculate the free energy of formation of a sharp interface (including vibrational contributions) using the effective cluster interactions at the appropriate temperature and a dividing surface construction. In this simplified geometry and with a perfect stoichiometry, the determination of the dividing surface that makes the excess solute zero is also especially simple. These simplifications turned out to be possible in the case of the Al_3Ti precipitates considered here as an example.

E. Parametrization of the Orientation Dependence

The interfacial excess free energy provided by Equation (2) is unfortunately not in a very convenient form. First, it is given numerically in tabular form on a mesh of possible directions. Second, it is contaminated by noise due to the fact that facets are rarely perfect (and in fact, are not perfect in general, due to the stabilizing effect of entropy) and due to ambiguities in defining the interface, as some solute atoms may be misclassified as part of the precipitate. The resulting interfacial free energies are thus not guaranteed to satisfy the symmetry constraints imposed by the crystallography of the problem. These problems can be jointly addressed by fitting the raw output of Equation (2) to a small set of direction-dependent harmonics that are adapted to the known symmetry of the precipitate’s crystal structure. We now describe a simple and general method to generate appropriate harmonics which exploits a convenient characterization of spherical harmonics as polynomials in the components of a unit vector.

Suitable treatments for special cases already exist in the literature. Notable examples include the cubic harmonics (e.g.^{48,49}) and harmonics for hexagonal symmetry (e.g.^{50,51}). A very general treatment has already been presented in the literature⁵². Although very complete, this treatment does not lend itself to a simple implementation: The point group and its orientation has to be identified, not just as a list of symmetry operations, but recognized by name as one

of the known point groups, so that one can lookup the specific rules applying to that point group. Based on the point group category found (e.g., cubic or hexagonal), a superset of harmonics is selected. Then, based on the specific point group found, “index rules” are applied to eliminate those harmonics that should vanish by symmetry. This treatment is ideally suited for researchers wanting to manually construct a basis based on the knowledge of the point group, as the different cases are nicely classified by point group. However, a computer program implementing the method would also necessarily contain a large number of tests and subcases. It would also have to rotate the symmetries into a standard “setting” to use the tabulated index rules. Moreover, if one wishes to handle other point groups that are not special cases of cubic or hexagonal symmetries (e.g. icosahedral symmetry or other noncrystallographic point groups, which could occur for quasicrystals), a different superset of harmonics and index rules must be constructed.

In contrast, we describe here an approach that works directly with the symmetry operation in matrix form (which are easy to determine) and requires no classification into categories of point groups. The possibility of having point groups in different orientations (or “settings”) is automatically handled, with no extra coding effort. The algorithm only relies on basic linear algebra operations and handles any point group, not just those for which supersets of harmonics have already been constructed. The proposed method is related to the one proposed in⁵³ to generate tensor bases, although additional steps, provided herein, were needed to formally show that such tensors bases can be used to generate direction-dependent harmonics and to avoid redundant harmonics via a projection scheme.

While we outline the method below, a formal algorithm is given in Appendix A 1. Polynomials are known to form a complete basis for any continuous function over a bounded region (e.g. the unit sphere). Hence, in particular, they form a complete basis for any continuous function defined over the surface of the unit sphere. Let u be a three-dimensional unit vector (e.g. $u = (\cos(\theta)\sin(\phi), \sin(\theta)\sin(\phi), \cos(\phi))$). Any continuous function f of direction u can therefore be represented as

$$f(u) = \sum_{L=0}^{\infty} A^{(L)} u^L \quad (4)$$

where we use the short-hand notation

$$A^{(L)} u^L \equiv \sum_{i_1=1}^3 \cdots \sum_{i_L=1}^3 A_{i_1 \cdots i_L}^{(L)} \prod_{j=1}^L u_{i_j} \quad (5)$$

(with $A^{(0)} u^0$ defined as constant) and where $A_{i_1 \cdots i_L}^{(L)}$ is a rank L tensor that is symmetric under permutation of the indices (since permutations of the indices does not change the polynomial we can, without loss of generality, limit ourselves to such symmetric tensors). If the function $f(u)$ is constrained by symmetry, such constraints can then be implemented by restricting the tensors $A^{(L)}$ to obey suitable invariance with respect to all symmetry operations in a given point group⁵⁴. As explained in more detail in the Appendix A 1, this can be simply accomplished by considering 3^L noncolinear trial tensors, and obtaining symmetrized tensors by averaging each trial tensor with all its transformations by each point group symmetry operation. The desired result is obtained after eliminating colinear symmetrized tensors.

An additional step is needed because expansion (4) is a bit redundant, since the polynomial $(u_1^2 + u_2^2 + u_3^2)$ is constant over the unit sphere. This would imply that nonzero coefficients $A^{(L)}$ for $L > 0$ could give rise to a constant $f(u)$, which is undesirable. This can be avoided by projecting each $A^{(L)}$ onto the space orthogonal to tensors giving rise to polynomials that can be factored as

$$(u_1^2 + u_2^2 + u_3^2) A^{(L-2)} u^{L-2} \quad (6)$$

for some tensor $A^{(L-2)}$ of rank $L - 2$. (It is not necessary to consider higher powers of $(u_1^2 + u_2^2 + u_3^2)$ in this factorization, because $A^{(L-2)} u^{L-2}$ could include additional $(u_1^2 + u_2^2 + u_3^2)$ factors as a special case.) A simple algorithm to accomplish the symmetrization and this projection is provided in Appendix A 1.

The result of this procedure is an expression for the tensor $A^{(L)}$ as a sum of K_L symmetry-constrained and non-redundant components $A^{(L,k)}$:

$$A^{(L)} = \sum_{k=1}^{K_L} c_{L,k} A^{(L,k)}$$

where the tensors $A^{(L,k)}$ are fixed and determined by symmetry while the coefficients $c_{L,k}$ are completely unrestricted. Upon substitution into (4) we obtain a symmetry-constrained expansion:

$$f(u) = \sum_{L=0}^{\infty} \sum_{k=1}^{K_L} c_{L,k} A^{(L,k)} u^L. \quad (7)$$

It is instructive to verify that expansion (7) coincides (apart from an inconsequential linear transformation) with spherical harmonics when no symmetry constraints are imposed. The easiest way to see this is to compare (7) with the eigenfunction of the Schrödinger equation for some spherically symmetric potential selected so that the eigenfunctions involve polynomials. We can use any convenient radial potential because we only focus on the angular part. Consider a spherically symmetric harmonic potential, whose eigenstates are polynomials times a spherically symmetric Gaussian. The Gaussian is constant over the unit sphere, so we are left with only a polynomial as the angular dependence. Moreover, it is well-known that the order of that polynomial is equal to $n_1 + n_2 + n_3$, the sum of three principal quantum numbers of the harmonic oscillator along each dimension. This sum is also (up to a constant scaling and shift) the energy of the system. It follows that there is a direct correspondence between all terms in (7) sharing the same value of L and all eigenfunctions sharing the same energy. The different terms sharing the same L thus correspond to eigenstates with different angular momentum projections. We can verify that the number of terms (in the case of a spherically symmetric potential) matches the number of spherical harmonics for a given value of L . Indeed, the number of distinct terms of total power L in a polynomial in v variables is $\binom{L+2}{v-1}$. In the present case $\binom{L+2}{3-1} = (L+2)(L+1)/2$. From that number, we subtract the dimension of the subspace of polynomials that factor as $(u_1^2 + u_2^2 + u_3^2)$ times a polynomial of order $L-2$, we obtain $\binom{L+2}{2} - \binom{L}{2} = (L+2)(L+1)/2 - L(L-1)/2 = 2L+1$, exactly the number of spherical harmonics associated with angular momentum is L . Hence the dimension of the space spanned by the spherical harmonics for a given L is the same as the dimension of the space spanned by our polynomials. Both spaces include polynomials of order L on the unit sphere that are not colinear and it follows that both bases must span the same space. Hence both expansions, truncated to the same L , span the same space.

The algorithm proposed above has been implemented within the Alloy Theoretic Automated Toolkit (ATAT)^{21,31–33} as the “gencs” code, documented in Section C. For convenience, the coefficients $A^{(L)}$ (up to $L=6$) for all crystallographic and selected noncrystallographic point groups can also be found in electronic form in the Supplementary Material (**suppmat.txt**). Figure 2 represents these harmonics graphically for each of the crystallographic point groups. Figure 3 shows the result of a similar exercise for selected noncrystallographic point groups, which could be useful, for instance, to handle the case of quasicrystals precipitating out of a liquid.

III. RESULTS

A. Cluster expansion

Since our focus is in the equilibrium between an Al-rich solid solution and Al_3Ti precipitate, the range of composition sampled during the cluster expansion construction process was restricted to less than 30 atomic percent Ti. Agreement between the ground state convex hulls from the raw DFT energies and the energies obtained from the cluster expansion (see Figure 4) was enforced in the range of 0 to 25 atomic percent Ti. Restricting the composition range in this fashion drastically improves the convergence of the cluster expansion. The cluster expansion construction process necessitated the calculation of the formation of energy, using ab initio methods, of 21 structures ranging from 1 to 12 atoms per unit cell. The ground state search was extended up to 12 atoms per unit cells. The resulting cluster expansion exhibits a mean square error of 15 meV. In this system, only pair interactions were found to be necessary, as determined from a cross-validation analysis²¹. These interactions are depicted in Figure 5.

The temperature dependence of these interactions was calculated via the transferable force constant approach (also called the “bond stiffness vs bond length” approach)^{40,41}. Three structures were used in the fit of the force constants (pure Al, Al_3Ti in the DO_{23} structure and a metastable Al_7Ti_3 structure with 10 atoms per unit cell, chosen for its small size and the presence of Ti-Ti bounds) and each were considered at their equilibrium lattice parameters at 0K as well as under a linear strain of 2%. The resulting length-dependence of the force constants is illustrated in Figure 6, along with the input ab initio stiffness data. These ab initio phonon calculations were performed using supercells ranging from 32 to 48 atoms, which is sufficient given the nearest-neighbor nature of the transferable force constants. These transferable length-dependent force constants were then used to calculate phonon spectra for all 21 structures used in the cluster expansion construction. A cross-validation analysis indicated that the configuration-dependence of the phonon free energy can be captured using only the 3 nearest neighbors pairs in the cluster expansion. Although the temperature-dependence of the interactions (Figure 5) may appear small, it nevertheless has a significant impact on the temperature scale of thermodynamics of the system. In precipitation calculations neglecting the effect of phonons (not described here, for conciseness), the precipitate exhibited flat facets up to around 1500K, while roughening occurs below 900K when vibrational effects are included.

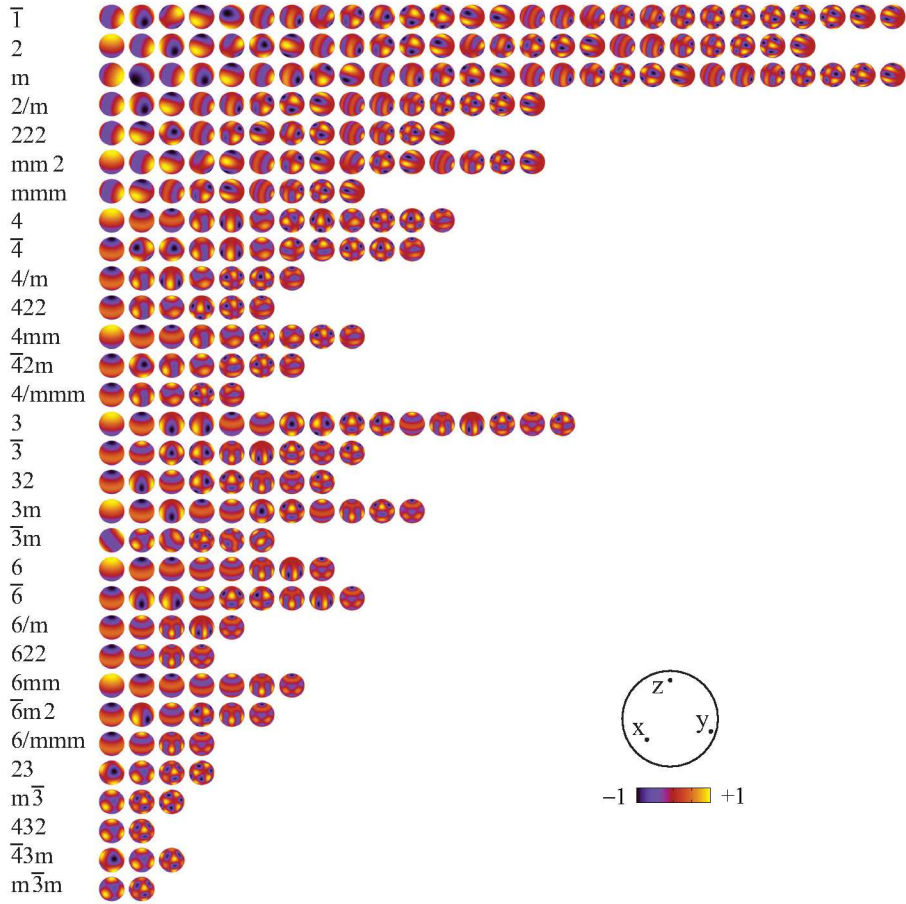


FIG. 2: (Color online) Symmetry-adapted spherical harmonics for each crystallographic point groups (up to $L=6$). Group 1 (with 48 harmonics) is omitted. The inset shows the location of the Cartesian axes on the unit sphere (where directions of highest symmetry are aligned, whenever possible) and the color scheme used to represent the function. Unique axis (when appropriate) is chosen to be z .

B. Monte Carlo simulations

Canonical Monte Carlo simulations were performed with the “emc2” code⁵⁵ included in ATAT which implements a standard Metropolis algorithm. Two types of simulations were used: (i) planar interface simulations, to obtain one absolute excess free energy and (ii) precipitate shape equilibration simulations, to obtain the relative excess free energies for all interface directions.

The planar interface simulations were performed in a $12 \times 12 \times n$ supercells of the cubic conventional cell of fcc, with $n = 18, 24, 30$. The supercell consisted of 1/2 Al₃Ti and 1/2 pure Al, resulting in two {001} interfaces. During the thermodynamic integration runs, we observed that the {001} interfaces remained atomically flat up to 900K, thus suggesting that configurational contribution to the interfacial excess are negligible and that thermodynamic integration is unnecessary. It was verified that this finding was not merely an artifact of insufficient equilibration, by deliberately starting the simulation with an excess solute dissolved in the host phase and observing that these solutes rapidly attach to the surface, one layer at a time and remain in place for the duration of the simulation. Given this behavior, we report here the excess free energy of a perfectly flat {001} interface obtained directly from the cluster expansion (which agrees, within numerical integration noise, with the full thermodynamic integration results). The interfacial excess free energy of the {001} interfaces at 900K is 240 mJ/m², using a dividing surface that makes the

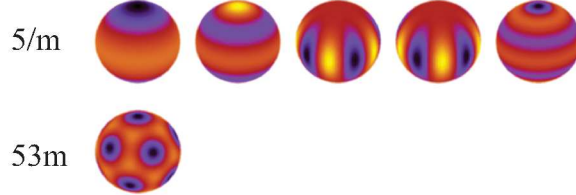


FIG. 3: (Color online) Symmetry-adapted spherical harmonics for selected noncrystallographic point groups (up to L=6), represented using the same conventions as in Figure 2.

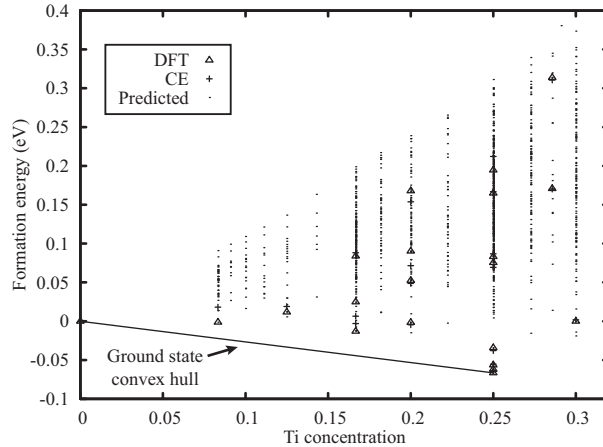


FIG. 4: Calculated DFT formation energies (triangles) and corresponding energies from the fitted cluster expansion (crosses). Dots mark predicted energies of structures not included in the fit. The line marks the convex hull of the ground state energies.

interfacial excess solute (Ti) vanish. Areas are calculated assuming the lattice parameter of pure Al, corresponding to the limit of small coherent precipitates in a dilute solid solution. This is the relevant limit since the concentration of Ti solutes in the host phase (fcc Al) was found to be less than 10^{-4} .

To verify convergence of the result with respect to precipitate size, we performed simulations for a range of precipitate sizes. The simulation cells considered were $n \times n \times n$ supercells of the cubic conventional cell of fcc with $n = 24, 36, 48, 60$. In each case, the precipitate was a parallelepiped occupying 2/3 of the simulation supercell along each direction (to ensure that the precipitate does not interact with its periodic images). These correspond to simulations involving from $\sim 55,000$ to 864000 atoms with precipitates containing from $\sim 12,000$ to $\sim 225,000$ atoms. In each case, the precipitate was first equilibrated for at least 10,000 Monte Carlo passes at the higher temperature of 1800K (to speed up the process) before being equilibrated at the final temperature of interest 900K for at least 16,000 passes. The inverse Wulff construction were performed on 10 snapshots separated by 1000 Monte Carlo passes and averaged to yield the data reported here. In a medium-sized supercell ($36 \times 36 \times 36$), it was verified that the simulation

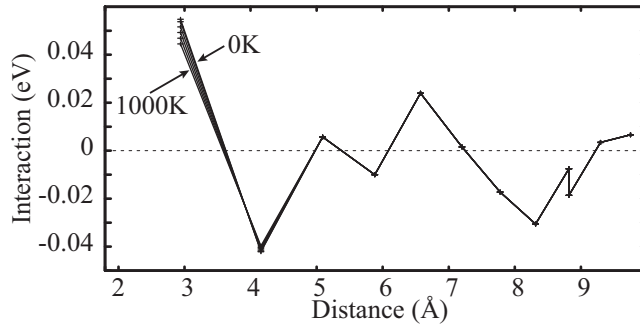


FIG. 5: Effective interaction $J_{...}$ as a function of distance.

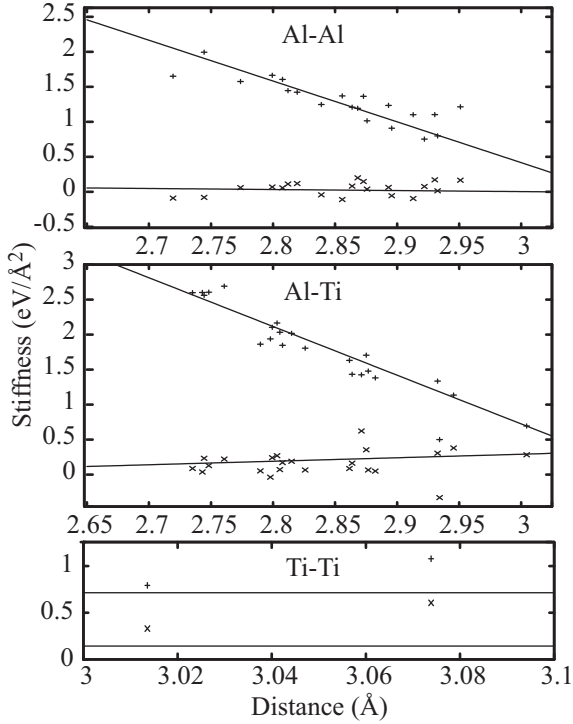


FIG. 6: Stiffness vs. Length relationship obtained from a fit to three structures and used to efficiently calculate the phonon spectrum for a large number of structures. Stiffness data for bond stretching and bending are marked by “+” and “×”, respectively. The resulting linear fits are used in subsequent phonon calculations.

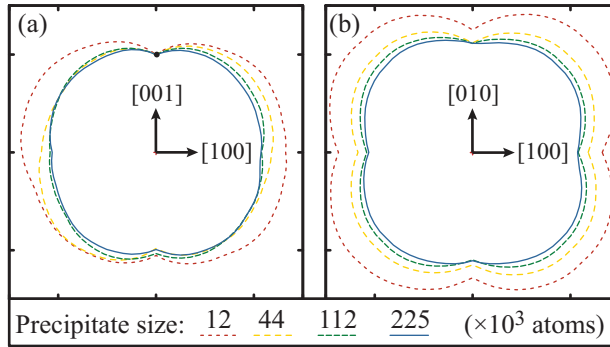


FIG. 7: (Color online) Convergence of the direction-dependence of the interfacial free energy $\tilde{\gamma}(u)$ as a function of precipitate size along two planar cross-sections. $\tilde{\gamma}(u)$ is normalized so that $\tilde{\gamma}((0, 0, 1)) = 1$, as indicated by the black circle. These plots show the unprocessed data, prior to a fit to harmonics (hence deviations from symmetry can be seen).

equilibrated to similar shapes even when starting from different initial solute shape: (i) an octahedron made of {111} facets and with longest axis of length 32 and (ii) a $24 \times 24 \times 12$ parallelepiped. The resulting equilibrium shape did not detectably change upon further equilibration for another 50,000 Monte Carlo passes at 900K.

Figure 7 show the convergence of the direction-dependence of the interfacial free energies obtained directly from the precipitate shape prior to a fit with harmonics. At small precipitate sizes, one can both see a systematic bias (due to the Gibbs-Thomson effect) and significant random noise (due to the resolution limit implied by the lattice parameter). The difference between the results obtained with the two largest precipitate sizes never differ by more than 5%, which can be taken as an upper bound on the magnitude of the errors.

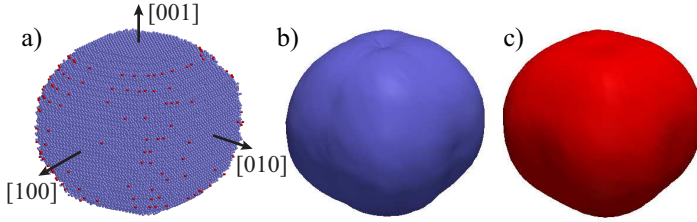


FIG. 8: (Color online) (a) Equilibrated Al_3Ti DO_{23} precipitate (at 900K) consisting of approximately 225,000 atoms (only Ti atoms are shown). Atoms identified as solute are marked in red. Note the combination of atomically flat $\{001\}$ facets and roughened interfaces in other directions. (b) Inverse Wulff construction from the precipitate shape that provides the relative interfacial excess free energy as a function of direction (units are dimensionless). (c) Symmetry-constrained harmonic expansion fitted to the data in b).

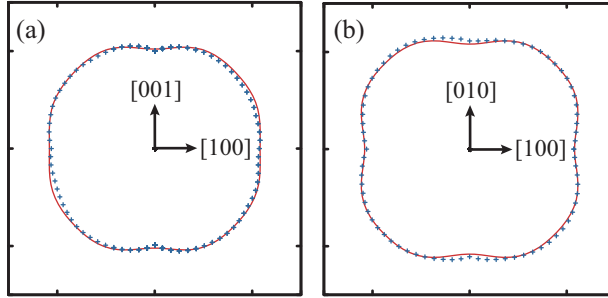


FIG. 9: (Color online) Panels (a) and (b) overlap the raw data (blue crosses) from the inverse Wulff construction (from Figure 7 for the largest precipitate size) and the least squares fit of a harmonic expansion (red continuous curve), along two planar cross-sections.

C. Interfacial excess free energies

The resulting equilibrium precipitate shape was fed to the inverse Wulff construction (Equation (2)), after the few solute atoms present in the Al matrix were eliminated by removing all Ti atoms no more than 2 Ti neighbors within a 5.1 Å radius. As illustrated in Figure 8, the Wulff plot obtained in this fashion is slightly noisy, but a least square fit to symmetry-constrained harmonics yield a well-behaved Wulff plot $\tilde{\gamma}(u)$ obeying the underlying symmetry of the DO_{23} phase ($4/mmm$). Cross-sections of the inverse Wulff construction are shown in Figure 9 along with their corresponding harmonic fits.

When facetting occurs, the Wulff plot $\gamma(u)$ contains nonsmooth cusps in the direction of the facets which may be difficult to represent with only a few smooth harmonics. However, it is easy to generate as many data points (i.e. directions u) as needed and as many harmonics as needed to alleviate this potential problem. In the present setting, including harmonics up to $L = 8$ and sampling the unit sphere on a grid of 40 different latitudes and 80 different longitudes was found to be sufficient for this purpose. It was found helpful to increase the weight of points near the cusp during the fit to ensure it is better reproduced. In the present system, a direction at an angle ϕ from the $[001]$ axis was given a weight of $\omega + (1 - \omega) \sin \phi$ with $\omega = 0.2$. (A uniform weight would have been of the form $\sin \phi$, but the additional ω term increases the weight near the cusp at $\phi = 0$.)

The resulting calculated interfacial excess free energies are reported in Table I, as a linear combination of these symmetry-constrained harmonics. The statistical noise (arising from the random fluctuations visible in Figure 9) introduce errors in the calculated free energies that are less than 1% and are thus negligible relative the precipitate size convergence errors (at most 5%). Excess free energies along selected directions, calculated from these harmonics, are also reported in Table II.

IV. CONCLUSION

Apart from a scaling constant, the complete orientation-dependence of interface free energies can be inferred from equilibrium precipitate shapes via the inverse Wulff construction. The scaling constant can be recovered from a calculation of the excess free energy of a single, conveniently chosen, planar interface, from a thermodynamic integration

TABLE I: Harmonic expansion (Equations (7) and (5)) of the calculated interfacial excess free energies. Harmonics are expressed in terms of the components (x, y, z) of a unit vector u . The number of significant digits reported reflects the standard errors of the statistical regression (1–5 mJ/m²). Finite size effects introduce an additional error of at most 5%.

Coefficient $c_{L,k}$	Value (mJ/m ²)	Harmonics $A^{(L,k)} u^L$
$c_{0,1}$	282	1
$c_{2,1}$	18	$0.408x^2 + 0.408y^2 - 0.816z^2$
$c_{4,1}$	-59	$0.396x^4 - 1.730x^2y^2 + 0.396y^4 - 0.649x^2z^2 - 0.649y^2z^2 + 0.216z^4$
$c_{4,2}$	2	$1.279x^2y^2 - 1.279x^2z^2 - 1.279y^2z^2 + 0.426z^4$
$c_{6,1}$	14	$0.154x^6 - 0.421x^4y^2 - 0.421x^2y^4 + 0.154y^6 - 1.894x^4z^2 + 5.050x^2y^2z^2 - 1.894y^4z^2 + 1.052x^2z^4 + 1.052y^2z^4 - 0.140z^6$
$c_{6,2}$	6	$0.557x^4y^2 + 0.557x^2y^4 - 0.557x^4z^2 - 6.680x^2y^2z^2 - 0.557y^4z^2 + 1.670x^2z^4 + 1.670y^2z^4 - 0.223z^6$
$c_{8,1}$	-73	$0.113x^8 - 2.011x^6y^2 + 4.640x^4y^4 - 2.011x^2y^6 + 0.113y^8 - 1.141x^6z^2 + 2.320x^4y^2z^2 + 2.320x^2y^4z^2 - 1.141y^6z^2 + 2.465x^4z^4 - 4.640x^2y^2z^4 + 2.465y^4z^4 - 0.677x^2z^6 - 0.677y^2z^6 + 0.0483z^8$
$c_{8,2}$	-9	$1.470x^6y^2 - 3.956x^4y^4 + 1.470x^2y^6 - 1.470x^6z^2 + 1.686x^4y^2z^2 + 1.686x^2y^4z^2 - 1.470y^6z^2 + 3.394x^4z^4 - 3.371x^2y^2z^4 + 3.394y^4z^4 - 1.133x^2z^6 - 1.133y^2z^6 + 0.0809z^8$
$c_{8,3}$	-27	$1.224x^4y^4 - 7.345x^4y^2z^2 - 7.345x^2y^4z^2 + 1.224x^4z^4 + 14.689x^2y^2z^4 + 1.224y^4z^4 - 1.469x^2z^6 - 1.469y^2z^6 + 0.105z^8$

TABLE II: Calculated interfacial excess free energies along selected directions (within an accuracy of 5%, due to finite size effects).

Direction	Interfacial Free energy (mJ/m ²)
{0 0 1}	245
{1 0 0}	259
{1 1 0}	268
{1 0 1}	206
{1 1 1}	227

procedure starting from a sharp interface at absolute zero.

The present work goes beyond these simple realizations along many key aspects. We employ the cluster expansion formalism in its most general coarse-graining form to efficiently model the system's energetics in a way that includes the effect of lattice vibrations without necessitating explicit modeling of the atomic dynamics throughout the simulation. This approach provides sufficient efficiency to reach the simulation system sizes and the equilibration times needed to obtain properly equilibrated precipitates of a size sufficient to enable the reliable determination of their shapes. The method is able to account for essentially all sources of entropy (arising from phonons, bulk point defects, as well as interface roughness) and is thus able to transparently handle both atomically smooth and rough interfaces. This feature is illustrated by an application to precipitates in the Al-Ti alloy system.

We also address the conceptual issue that some interface directions do not appear on the Wulff shape when facetting occurs. We show how the interfacial free energy surface can be naturally extended into the “masked” regions of the Wulff plot in a way that (i) preserves the predicted equilibrium shape and (ii) has a natural geometric interpretation.

We provide symmetry-adapted harmonic bases (both in the form of a simple algorithm and as explicit expressions for all crystallographic point groups) to represent the resulting orientation-dependent interfacial free energies. The same bases could prove more generally useful in a variety of other applications, for instance to represent the anisotropy of the so-called constituent strain elastic energy.

Acknowledgements

This work is supported by XSEDE computing resources and by the National Science Foundation under Grant No. DMR-0907669.

Appendix A: Harmonic generation method

1. Definitions

Let us first define a few convenient symbols.

- Let S denote a 3×3 matrix representing a point symmetry operation in Cartesian coordinates and let the corresponding function $S(A^{(L)})$ applied to a tensor $A^{(L)}$ of rank L be defined as:

$$[S(A^{(L)})]_{j_1, \dots, j_L} = \sum_{i_1=1}^3 \cdots \sum_{i_L=1}^3 A_{i_1, \dots, i_L}^{(L)} \prod_{k=1}^L S_{i_k j_k}$$

and let \mathcal{S} denote a set of such matrices that defines the point group of interest.

- Let P denote a permutation vector (i.e. an L -dimensional vector containing all the numbers $\{1, \dots, L\}$ not necessarily in increasing order) and let the function $P(\cdot)$ be defined as:

$$[P(A^{(L)})]_{j_1, \dots, j_L} = A_{i_{P(1)}, \dots, i_{P(L)}}^{(L)}$$

and let $\mathcal{P}^{(L)}$ denote the set of all such permutations for a given L .

- Let $\#\#$ denote the number of elements in a set.
- Let $C^{(L,1)}, \dots, C^{(L,M)}$ be a set of rank L tensors defining linear constraints on the generated tensor basis, i.e. the $A^{(L,k)}$ generated must be orthogonal to all $C^{(L,m)}$, according to the inner product

$$A^{(L,k)} \cdot C^{(L,m)} \equiv \sum_{i_1=1}^3 \cdots \sum_{i_L=1}^3 A_{i_1, \dots, i_L}^{(L,k)} C_{i_1, \dots, i_L}^{(L,m)}. \quad (\text{A1})$$

(If $M = 0$, no constraints are imposed.)

- Let $\text{vec}(A^{(L)})$ denote a vectorization of the tensor $A^{(L)}$ (i.e. a 3^L -dimensional column vector containing all elements of the tensor $A^{(L)}$) and let $\text{unvec}(\cdot)$ denote the reverse operation.

2. Algorithm

Our algorithm for generating a basis for tensors of rank L obeying symmetric constraints (defined by a point group \mathcal{S}), indices permutation invariance constraints (defined by the set $\mathcal{P}^{(L)}$) and some linear constraints (defined by a basis of symmetric (under index permutations) tensors $C^{(L,1)}, \dots, C^{(L,M)}$) is then as follows:

1. If $M > 0$, define B to be the nonzero and non linearly dependent columns of the matrix:

$$B = [\text{vec}(C^{(L,1)}), \dots, \text{vec}(C^{(L,M)})].$$

2. Set $k = 0$
3. Consider a set of distinct trial tensors $\tilde{A}^{(L,t)}$ for $t = 1, \dots, 3^L$, each consisting of a single element set to 1, with all remaining elements set to 0 and set

$$A^{(L,t)} = \frac{1}{\#\mathcal{P}} \sum_{P \in \mathcal{P}} P(\tilde{A}^{(L,t)}).$$

(For added efficiency, one can limit the trial tensors to those whose nonzero element $\tilde{A}_{i_1, \dots, i_L}$ obeys $i_1 \leq i_2 \leq \dots \leq i_L$. Also, it is clear that the sum over permutations \mathcal{P} is just equivalent to setting to 1 all elements of the tensor $A^{(L,t)}$ equivalent to the nonzero element of $\tilde{A}^{(L,t)}$ under index permutations.)

(a) For each trial tensor $A^{(L,t)}$, set

$$Q = \text{unvec} \left(\left(I - B (B^T B)^{-1} B^T \right) \text{vec} \left(A^{(L,t)} \right) \right)$$

(or simply $Q = A^{(L,t)}$ if $M = 0$).

(b) Calculate

$$\bar{Q} = \frac{1}{\#\mathcal{S}} \sum_{S \in \mathcal{S}} S(Q)$$

(c) If \bar{Q} is nonzero (within machine numerical precision) and (for $k > 0$) not linearly dependent with the $[\bar{A}^{(L,1)}, \dots, \bar{A}^{(L,k)}]$, then increment k and set $\bar{A}^{(L,k)} = \bar{Q}$.

4. Finally, set $K_L = k$ and orthogonalize (and normalize) the element of $[\bar{A}^{(L,1)}, \dots, \bar{A}^{(L,K_L)}]$ using the Gram-Schmidt procedure.

The harmonics of order up to L^{\max} are then generated by calling the above routine for $L = 1, \dots, L^{\max}$, setting $M = 0$ if $L \leq 2$ and otherwise setting the constraints $C^{(L,k)}$ to be

$$\begin{aligned} C^{(L,k)} &= \sum_{P \in \mathcal{P}} P(\tilde{C}) \\ \text{with } \tilde{C}_{i_1, \dots, i_L} &= \delta_{i_1, i_2} \tilde{A}_{i_3, \dots, i_L}^{(L-2,k)} \end{aligned}$$

where the $\tilde{A}^{(L-2,k)}$ are also generated with the above routine, called with rank $L - 2$, the same point group \mathcal{S} , the permutation set $\mathcal{P}^{(L-2)}$ and $M = 0$ (no constraints $C^{(L-2,k)}$).

Although it is not explicit in the notation above, it is clear that efficiency improvements (in storage and computational requirements) are possible by exploiting, at each step, the symmetry of all tensors considered under permutation of their indices. However, for the basis sizes we considered in this paper, we found such optimization to be unnecessary. It is also interesting to note that, since all operations (except for the last normalization step) yield tensors with rational elements, one can use an exact rational representation for the coefficients to obtain an analytic (rather than numerical) expression for the harmonics. We did not find this to be necessary, however, and, in fact, harmonics are often reported in numerical form^{48,49}.

3. Proof of the validity of the symmetrization technique

It is instructive to see why the method used for symmetrization in the algorithm of Section A 1 actually works. For an arbitrary trial tensor $A^{(L,t)}$ we can verify that the symmetrized tensor

$$\tilde{Q} = \frac{1}{\#\mathcal{S}} \sum_{S \in \mathcal{S}} S(A^{(L,t)})$$

obeys $T(\tilde{Q}) = \tilde{Q}$ for any operation $T \in \mathcal{S}$. Indeed, calculate

$$T(\tilde{Q}) = \frac{1}{\#\mathcal{S}} \sum_{S \in \mathcal{S}} T(S(A^{(L,t)})) = \frac{1}{\#\mathcal{S}} \sum_{\tilde{S} \in \mathcal{S}} \tilde{S}(A^{(L,t)}) = \tilde{Q}$$

where the second equality holds because $T(S(\cdot))$ is just another operation in $\tilde{S}(\cdot) \in \mathcal{S}$ and two distinct $S(\cdot)$ cannot be mapped onto the same symmetry operation by applying $T(\cdot)$, since each element of a group admits an inverse. Since the symmetrization procedure is a linear projection, choosing the trial tensors $A^{(L,t)}$ so that they form an orthogonal basis is sufficient to generate a basis for the space of symmetrized tensors.

A similar argument holds for invariance under permutations P of the indices. Finally, note that applying a point group operation $S(\cdot)$ to a tensor $A^{(L)}$ that is invariant to indices permutations yields a tensor with the same property:

$$\begin{aligned}
[P(S(A^{(L)}))]_{j_1, \dots, j_L} &= [S(A^{(L)})]_{j(P_1), \dots, j(P_L)} = \sum_{i_1=1}^3 \dots \sum_{i_L=1}^3 A_{i_1, \dots, i_L}^{(L)} \prod_{k=1}^L S_{i_k j_{P(k)}} \\
&= \sum_{i_1=1}^3 \dots \sum_{i_L=1}^3 A_{i_{P(1)}, \dots, i_{P(L)}}^{(L)} \prod_{k=1}^L S_{i_{P(k)}, j_{P(k)}} \\
&= \sum_{i_1=1}^3 \dots \sum_{i_L=1}^3 A_{i_{P(1)}, \dots, i_{P(L)}}^{(L)} \prod_{k=1}^L S_{i_k, j_k} \\
&= \sum_{i_1=1}^3 \dots \sum_{i_L=1}^3 A_{i_1, \dots, i_L}^{(L)} \prod_{k=1}^L S_{i_k, j_k} = [S(A^{(L)})]_{i_1, \dots, i_L}
\end{aligned}$$

where we have used the fact re-ordering the sums or the product has no effect and the invariance of $A^{(L)}$ under permutation. This shows that symmetrizing the tensor after making it invariant to indices permutations does not undo the permutation invariance.

Appendix B: Interpretation of nonequilibrium excess free energies

Let u be a unit vector and let $\gamma(u)$ denote the surface (free) energy for an interface with normal u . Consider an interface that appears macroscopically flat with normal u_0 and unit area $A_0 = 1$ but that is, microscopically made of K different facets of orientations u_1, \dots, u_K with corresponding areas A_1, \dots, A_k . We assume that these facets are big enough that the edge energies are negligible relative to the surface energies, but small enough that the interface still appears macroscopically flat. Our goal is to express the $\gamma(u_0)$ in terms of u_0, u_1, \dots, u_K and $\gamma(u_1), \dots, \gamma(u_K)$.

The first step is to solve for the A_1, \dots, A_K . To this effect, consider a uniform fictitious “field” f traversing the surface u_0 and observe that this flux must be equal to the flux traversing the faceted surface made of orientations u_1, \dots, u_K :

$$A_0 u_0 \cdot f = \sum_{k=1}^K A_k u_k \cdot f$$

Since this must hold for any constant flux f and since $A_0 = 1$ by convention, we have the vector identity $u_0 = \sum_{k=1}^K A_k u_k$ which can be written in matrix form as $Ua = u_0$ where $U = [u_1, \dots, u_K]$ and $a = [A_1, \dots, A_k]^T$. If $K = 3$, U is a 3×3 matrix that is necessarily invertible (for otherwise some facets would be redundant). If $K = 2$, the problem can be reduced to a two-dimensional problem by a change of coordinates and U is 2×2 matrix that is invertible. The $K = 1$ case is trivial. We can then generally solve for the A_k via $a = U^{-1}u_0$. The effective surface energy is then

$$\gamma(u_0) = \sum_{k=1}^K \gamma(u_k) A_k = g^T a = g^T U^{-1} u_0 \tag{B1}$$

where $g = [\gamma(u_1), \dots, \gamma(u_K)]^T$.

We can obtain the same answer via a simple geometric construction. Let x be the point of intersection of the facets of the Wulff shape associated with u_1, \dots, u_K . This point x can be found by solving the system of equations $u_k \cdot x = \gamma(u_k)$ for $k = 1, \dots, K$. which can be written in matrix form as $U^T x = g$, using the earlier notation. Hence, $x = (U^T)^{-1} g$. Now consider a plane with normal u_0 intersecting x . Its distance from the origin is given by

$$x^T u_0 = ((U^T)^{-1} g)^T u_0 = g^T U^{-1} u_0$$

which is exactly the same as $\gamma(u_0)$ given by (B1). This implies that the inverse Wulff construction automatically extrapolates the surface free energies to the “unstable” directions to reproduce the energy of a microscopically faceted surface made of equilibrium facets that are large enough to make edge energies negligible.

Appendix C: Supplementary Material: Using the gencs code

The code takes, as an input, either a point group (specified via generators) or a structural information from which it determines the point symmetry automatically. It outputs the harmonics in a file, in form that is easy to read into a computer code and outputs the harmonics in human-readable form on the standard output. Some of the file formats contain extraneous items not needed for harmonic generation *per se* (marked in italics below), but that are included to ensure compatibility with other portions of the ATAT package.

1. Input files

By default, the code reads in structural information (from the `lat.in` file by default — a alternate file name can be specified with the `-l` option) and determines the point group automatically. The `lat.in` file has the following format.

1. First, the coordinate system $\vec{a}, \vec{b}, \vec{c}$ is specified, either as

$$[a] [b] [c] [\alpha] [\beta] [\gamma]$$

or in terms of Cartesian coordinates, one axis per line:

$$\begin{bmatrix} a_x \\ b_x \\ c_x \end{bmatrix} \begin{bmatrix} a_y \\ b_y \\ c_y \end{bmatrix} \begin{bmatrix} a_z \\ b_z \\ c_z \end{bmatrix}$$

2. Then the lattice vectors $\vec{u}, \vec{v}, \vec{w}$ are listed, one per line, expressed in the coordinate system just defined:

$$\begin{bmatrix} u_a \\ v_a \\ w_a \end{bmatrix} \begin{bmatrix} u_b \\ v_b \\ w_b \end{bmatrix} \begin{bmatrix} u_c \\ v_c \\ w_c \end{bmatrix}$$

3. Finally, the position x_i and type(s) t_{1i}, t_{2i}, \dots of atom for site i are given, expressed in the same coordinate system as the lattice vectors:

$$\begin{bmatrix} x_{a1} & x_{b1} & x_{c1} & [t_{11}, t_{21}, \dots] \\ x_{a2} & x_{b2} & x_{c2} & [t_{12}, t_{22}, \dots] \\ \vdots & \vdots & \vdots & \vdots \end{bmatrix}$$

An example of such file, for an Al-Ti alloy adopting the hcp crystal structure is:

3.1 3.1 5.062 90 90 120	(Coordinate system: a b c α β γ notation)
1 0 0	(Primitive unit cell: one vector per line)
0 1 0	expressed in multiples of the above coordinate
0 0 1	system vectors)
0 0 0 Al,Ti	(Atoms in the lattice)
0.6666666 0.3333333 0.5 Al,Ti	

As an alternative to providing the above structural information, the user can provide generators of the point group (which could also be the whole point group) and the code will complete the full point group automatically. This input file is called `sym.in` and has the format:

```
[Number symmetry operations given as generators]
[3×3 matrix representing a symmetry operation in Cartesian coordinates]
0 0 0
[another 3×3 matrix representing a symmetry operation in Cartesian coordinates]
0 0 0
...

```

2. Output file

The harmonics are output in the file `harm.out`, which has the following format:
For each harmonic:

```

1
0
0
tensor
[rank]
[ $3^{\text{rank}}$  repeated 'rank' times]
[ $3^{\text{rank}}$ ]
[the  $3^{\text{rank}}$  elements of the tensor]
...

```

In addition, the standard output displays the harmonics in human-readable format, with x , y , z denoting the components of a unit vector.

3. Command line options

```

-l=[string] Input file defining the lattice (default: lat.in)
-s          Specify point group directly via generator (in sym.in)
-z=[real]   Tolerance for finding symmetry operations (default: 2e-4)
-r=[int]    Maximum Rank of the harmonic
-mr=[int]   Minimum Rank of the harmonic (default 1)
-sig=[int]  Number of significant digits printed (default: 5)

```

Invoking the code without any options displays help. At the minimum, the user must specify the `-r` option. All other options are optional.

* Electronic address: avdw@alum.mit.edu

¹ Y. Mishin and J. L. M. Asta, *Acta Mater.* **58**, 1117 (2010).

² D. Wolf and S. Yip, eds., *Materials interfaces: atomic level structure and properties*, vol. 1 (Chapman & Hall, London, 1992).

³ I. M. Lifshitz and V. Slyozov, *J. Phys. Chem. Sol.* **19**, 35 (1962).

⁴ H. A. Calderon, P. W. Voorhees, J. L. Murray, and G. Kostorz, *Acta metall. mater.* **42**, 991 (1994).

⁵ A. J. Ardell, *Interface Sci.* **3**, 119 (1995).

⁶ A. J. Ardell, *J. Mater. Sci.* **46**, 4832 (2011).

⁷ Y. Mishin, *Acta Materialia* **52**, 1451 (2004).

⁸ Z. Mao, C. Booth-Morrison, E. Plotnikov, and D. N. Seidman, *J Mater Sci* **47**, 7653 (2012).

⁹ A. J. Ardell and V. Ozolins, *Nat. Mater* **4**, 309 (2005).

¹⁰ M. Asta and J. J. Hoyt, *Acta Mater.* **48**, 1089 (2000).

¹¹ M. Asta, *Acta Mater.* **44**, 4131 (1996).

¹² C. Woodward, A. V. de Walle, M. Asta, and D. Trinkle, *Acta Mater.* **Under Revision** (2013).

¹³ S. Muller, C. Wolverton, L. W. Wang, and A. Zunger, *Europhysics Letters* **55**, 33 (2001).

¹⁴ J. M. Sanchez, F. Ducastelle, and D. Gratias, *Physica* **128A**, 334 (1984).

¹⁵ A. van de Walle and M. Asta, *Metallurgical and Materials Transactions A* **33A**, 735 (2002).

¹⁶ M. Asta, S. M. Foiles, and A. A. Quong, *Phys. Rev. B* **57**, 11265 (1998).

¹⁷ N. A. Zarkevich and D. D. Johnson, *Phys. Rev. B* **67**, 064104 (2003).

¹⁸ M. Asta, V. Ozolins, and C. Woodward, *JOM - J. Min. Met. Mat. S.* **53**, 16 (2001).

¹⁹ M. Sluiter and Y. Kawazoe, *Phys. Rev. B* **54**, 10381 (1996).

²⁰ A. van de Walle and D. Ellis, *Phys. Rev. Lett.* **98**, 266101 (2007).

²¹ A. van de Walle and G. Ceder, *J. Phase Equilib.* **23**, 348 (2002).

²² N. Moelans, B. Blanpain, and P. Wollants, *Calphad* **32**, 268 (2008).

²³ V. Vaithyanathan, C. Wolverton, and L. Q. Chen, *Phys. Rev. Lett.* **88**, 125503 (2002).

²⁴ V. Vaithyanathan, C. Wolverton, and L. Chen, *Acta Materialia* **52**, 2973 (2004).

²⁵ F. Roters, P. Eisenlohr, L. Hantcherli, D. Tjahjanto, T. Bieler, and D. Raabe, *Acta Materialia* **58**, 1152 (2010).

²⁶ G. Wulff, *Zeitschrift fur Krystallographie und Mineralogie* **34**, 449 (1901).

- ²⁷ M. von Laue, Zeitschrift fur Kristallographie **105**, 124 (1943).
- ²⁸ S. Khare, S. Kodambaka, D. Johnson, I. Petrov, and J. Greene, Surface Science **522**, 75 (2003).
- ²⁹ D. B. Laks, L. G. Ferreira, S. Froyen, and A. Zunger, Phys. Rev. B **46**, 12587 (1992).
- ³⁰ V. Ozolinš, C. Wolverton, and A. Zunger, Phys. Rev. B **57**, 4816 (1998).
- ³¹ A. van de Walle, M. Asta, and G. Ceder, Calphad **26**, 539 (2002).
- ³² A. van de Walle, Calphad **33**, 266 (2009).
- ³³ A. van de Walle, *The Alloy Theoretic Automated Toolkit (ATAT)* (2001), <http://alum.mit.edu/www/avdw/atat/>.
- ³⁴ A. van de Walle, JOM - J. Min. Met. Mat. S. **65**, 1523 (2013).
- ³⁵ A. van de Walle, G. Ghosh, and M. Asta, in *Applied Computational Materials Modeling: Theory, Simulation and Experiment*, edited by G. Bozzolo, R. Noebe, and P. Abel (Kluwer Academic Publishers, 2005).
- ³⁶ J. Z. Liu, G. Ghosh, A. van de Walle, and M. Asta, Phys. Rev. B **75**, 104117 (2007).
- ³⁷ D. de Fontaine, Solid State Phys. **47**, 33 (1994).
- ³⁸ A. Zunger, in *NATO ASI on Statics and Dynamics of Alloy Phase Transformation*, edited by P. E. Turchi and A. Gonis (Plenum Press, New York, 1994), vol. 319, p. 361.
- ³⁹ F. Ducastelle, *Order and Phase Stability in Alloys* (Elsevier Science, New York, 1991).
- ⁴⁰ A. van de Walle and G. Ceder, Rev. Mod. Phys. **74**, 11 (2002).
- ⁴¹ A. van de Walle and G. Ceder, Phys. Rev. B **61**, 5972 (2000).
- ⁴² G. Kresse and J. Furthmüller, Phys. Rev. B **54**, 11169 (1996).
- ⁴³ G. Kresse and J. Furthmüller, Comp. Mater. Sci. **6**, 15 (1996).
- ⁴⁴ G. Kresse and D. Joubert, Phys. Rev. B **59**, 1758 (1999).
- ⁴⁵ J. P. Perdew, K. Burke, and M. Ernzerhof, Phys. Rev. Lett. **77**, 3865 (1996).
- ⁴⁶ W. Thomson, Phil. Mag., series 4 **42**, 448 (1871).
- ⁴⁷ C. Lupis, *Chemical Thermodynamics of Materials* (Prentice Hall, New York, 1983).
- ⁴⁸ S. L. Altmann and A. P. Cracknell, Rev. Mod. Phys. **37**, 19 (1965).
- ⁴⁹ J. Muggli, J. of Applied Mathematics and Physics **23** (1972).
- ⁵⁰ S. L. Altmann and C. J. Bradley, Rev. Mod. Phys. **37**, 33 (1965).
- ⁵¹ C. Varney and G. L. W. Hart, TMS Lett. **1**, 35 (2004).
- ⁵² M. Kara and K. Kurki-Suonio, Acta Cryst. **A37**, 201 (1981).
- ⁵³ A. van de Walle, Nat. Mater. **7**, 455 (2008).
- ⁵⁴ J. F. Nye, *Physical Properties of Crystals: Their Representation by Tensors and Matrices* (Oxford University Press, USA, 1985).
- ⁵⁵ A. van de Walle and M. Asta, Model. Simul. Mater. Sc. **10**, 521 (2002).